

Direct Detection of Key Intermediates during the Product Release in Rhenium Bipyridine-Catalyzed CO₂ Reduction Reaction

Samir Chattopadhyay, Mun Hon Cheah, Reiner Lomoth, and Leif Hammarström*



Cite This: *ACS Catal.* 2024, 14, 16324–16334



Read Online

ACCESS |

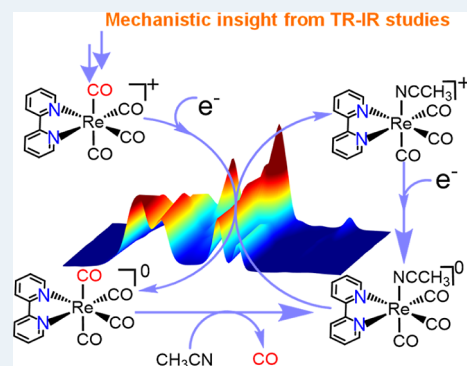
Metrics & More

Article Recommendations

Supporting Information

ABSTRACT: Rhenium bipyridine tricarbonyl complexes, $fac-[Re(bpy)(CO)_3X]^{n+}$, are highly effective in selectively converting CO₂ to CO under electrochemical and photochemical conditions. Despite numerous mechanistic studies aimed at understanding its CO₂ reduction reaction (CO₂RR) pathway, the intermediates further into the catalytic cycle have escaped detection, and the steps leading to product release remained elusive. In this study, employing stopped-flow mixing coupled with time-resolved infrared spectroscopy, we observed, for the first time, the reduced Re-tetracarbonyl species, $[Re(bpy)(CO)_4]^0$, with a half-life of approximately 55 ms in acetonitrile solvent. This intermediate is proposed to be common in both electrochemical and photochemical CO₂RR. Furthermore, we directly observed the release of the product (CO) from this intermediate. Additionally, we detected the accumulation of $[Re(bpy)(CO)_3(CH_3CN)]^+$ as a byproduct following product release, a significant side reaction under conditions with a limited supply of reducing equivalents mirroring photochemical conditions. The process could be unambiguously attributed to an electron transfer-catalyzed ligand substitution reaction involving $[Re(bpy)(CO)_4]^0$ by simultaneous real-time detection of all involved species. We believe that this side reaction significantly impacts the CO₂RR efficiency of this class of catalysts under photochemical conditions or during electrocatalysis at mild overpotentials.

KEYWORDS: CO₂ reduction reaction, molecular catalysts, time-resolved FTIR, stopped-flow mixing, reactive intermediates, CO release step, kinetic studies



INTRODUCTION

Electrochemical and photochemical CO₂ reduction (eCO₂RR/photo-CO₂RR) is a promising avenue for storing excess renewable energies or converting solar energy into valuable chemicals and fuels.^{1–4} Yet, CO₂ fixation faces challenges due to its high thermodynamic and kinetic stability,⁵ necessitating catalysts that employ multielectron/multiproton pathways to achieve CO₂ reduction reaction (CO₂RR) at moderate potentials.^{6–8} Additionally, the thermodynamic potentials for producing various 2e[−]/4e[−]/6e[−]/8e[−] CO₂RR products are close to each other, leading to a highly energy-intensive downstream separation process.^{9,10} Therefore, current catalyst development focuses on improving product selectivity in addition to the overpotential and electro-/photocatalytic rates.^{11–14}

Among a large library of molecular CO₂RR catalysts developed so far,^{15,16} rhenium (Re) bipyridine tricarbonyl chloride complex $fac-[Re(bpy)(CO)_3Cl]$ (where bpy is 2,2′-bipyridine) originally reported by Lehn and co-workers is one of the most efficient catalysts for the selective generation of CO from CO₂ under both electrochemical and photochemical conditions.^{17,18} Later, the research groups of Kubiak, Fujita, Ishitani, and others extensively studied the eCO₂R/photo-CO₂R reactivities of analogous Re complexes upon incorporat-

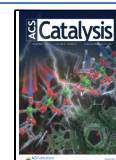
ing various functionalities onto the bipyridine framework, by replacing bipyridine moiety with phenanthroline, carbene-based ligands, and by coupling it with Ru-based photosensitizers, etc., which help in increasing the activity of the catalysts in terms of overpotentials and turnover numbers.^{19–21} Currently, there is an ongoing quest to bind this catalyst onto silicon photocathodes^{22–25} to construct artificial photosynthetic systems for selective CO₂RR integrated with water/waste oxidation reactions.²⁶ This catalyst also finds its place in tandem catalytic systems where the released CO is either reduced further by a nearby catalytic site to produce higher reduced products²⁷ or can directly be used in (radio)-carbonylation reactions to produce pharmaceutically relevant compounds.²⁸ This reflects the broad applicability of this evergreen catalyst in the development of efficient artificial photosynthetic systems. However, to tune the catalytic rate further and possibly change the product selectivity, a clear

Received: October 1, 2024

Revised: October 10, 2024

Accepted: October 10, 2024

Published: October 22, 2024



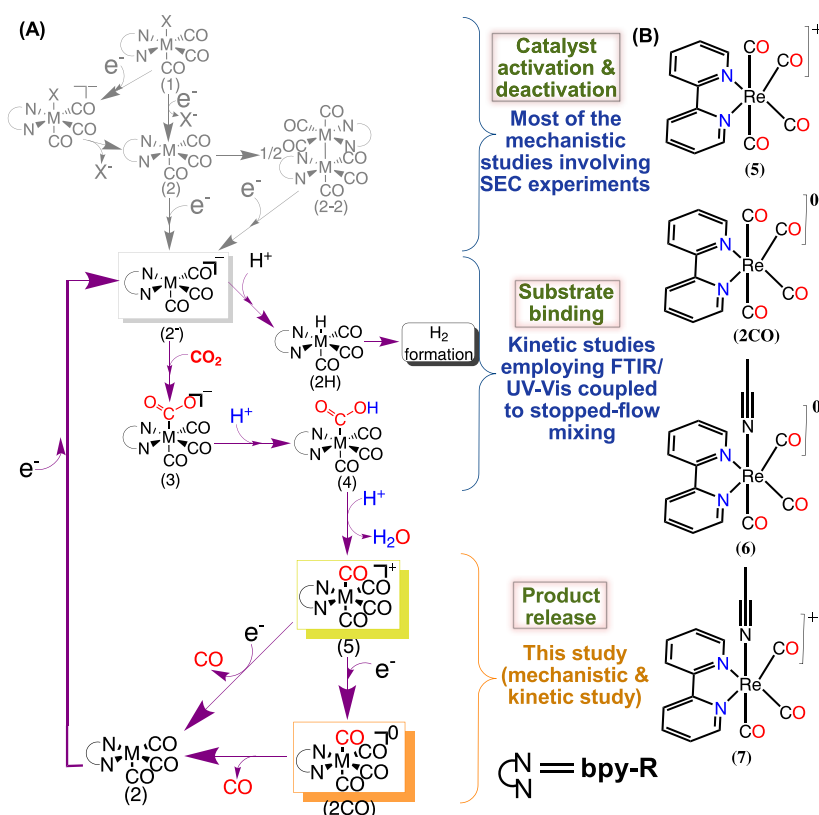


Figure 1. (A) Proposed mechanistic cycle of $e\text{CO}_2\text{RR}$ catalyzed by the $\text{M}(\text{bpy-R})(\text{CO})_3\text{X}$ complex, where $\text{M} = \text{Re}/\text{Mn}$, $\text{bpy} = 2,2'$ bipyridine, $\text{R} = \text{H}/\text{other functional groups}$, and $\text{X} = \text{Cl}/\text{Br}$.³¹ Here, we highlighted the current progress in mechanistic and kinetic studies done with these systems and how our current work will complement a complete understanding of the catalytic cycle. (B) Chemical structures of the species (intermediates) that are discussed in this paper.

understanding of the corresponding mechanistic cycle is well-sought. In situ spectroelectrochemical techniques, particularly FTIR, have evolved as an important tool to devise a plausible mechanistic cycle by observing some intermediates.^{19,29} A generic $e\text{CO}_2\text{RR}$ mechanistic cycle has been proposed for these types of catalysts using a combined experimental and computational approach (Figure 1A).^{30,31} The mechanism of photo- CO_2RR is slightly different in terms of the CO_2 binding intermediate, (vide infra, Scheme 2).³² Although numerous mechanistic studies were done to understand and devise a possible catalytic cycle, mainly employing FTIR-SEC, most of them were confined to the catalyst's activation and its possible deactivation pathways.³³ Publications that report the detection of the intermediates beyond the first species of the catalytic cycle (2^- , Figure 1) are scarce^{34,35} as the simultaneous accumulation of various species can hamper their detection in situ. A good approach would be to prepare intermediates (if sufficiently stable), study their reaction with electrons, substrates, and protons separately or in combination, and map the entire catalytic cycle step by step. To the best of our knowledge, there are only two kinetic studies reported in the literature to date, adopting this strategy, that deal with the binding kinetics of CO_2/H^+ to the first species of the catalytic cycle (2^- , Figure 1).^{36,37} This helps in going further into the catalytic cycle by observing the substrate binding. However, the product release part of the catalytic cycle remained elusive because the intermediates are short-lived³⁸ and escaped detection by the regularly employed methods, having lower time resolution.

Another challenge of studying the $e\text{CO}_2\text{RR}$ and photo- CO_2RR mechanisms lies in the scarcity of spectroscopic tools that could mimic both electrocatalytic conditions (unrestricted supply of electrons) and photocatalytic conditions (limited supply of reducing equivalents). Therefore, most of the intermediates predicted in the photo- CO_2RR mechanistic cycle were derived from the FTIR-SEC experiments²⁸ although the solvents used in these two cases are different (acetonitrile, CH_3CN in $e\text{CO}_2\text{RR}$ and dimethylformamide, DMF in photo- CO_2RR) and the exact reason behind the poor performance of these class of catalysts in CH_3CN under photochemical conditions is still unclear.²¹ Keeping all of these things in mind, we were motivated to explore the product release steps of the CO_2RR catalytic cycle (Figure 1 and Scheme 2) in CH_3CN .

Herein, we report detailed mechanistic and kinetic studies of the product (CO) release step of $e\text{CO}_2\text{RR}/\text{photo-CO}_2\text{RR}$ under pure chemical conditions employing time-resolved FTIR [time-resolved infrared spectroscopy (TRIR)] coupled to stopped-flow mixing. The reaction was initiated by bimolecular electron transfer from decamethyl cobaltocene (CoCp_2^*) to the catalytic intermediate, $[\text{Re}(\text{bpy})(\text{CO})_4]^+$ (5, Figure 1), which can be accessed synthetically. To the best of our knowledge, this study provides the first report of the observation of the 2CO intermediate ($[\text{Re}(\text{bpy})(\text{CO})_4]^0$), a common species predicted to be involved in both $e\text{CO}_2\text{RR}$ and photo- CO_2RR . The observation of direct product (CO) release from 2CO testifies that it is indeed the CO-releasing intermediate in both $e\text{CO}_2\text{RR}$ and photo- CO_2RR . We have also observed an electron-transfer-catalyzed ligand substitution reaction, and its implications for the catalytic cycle are

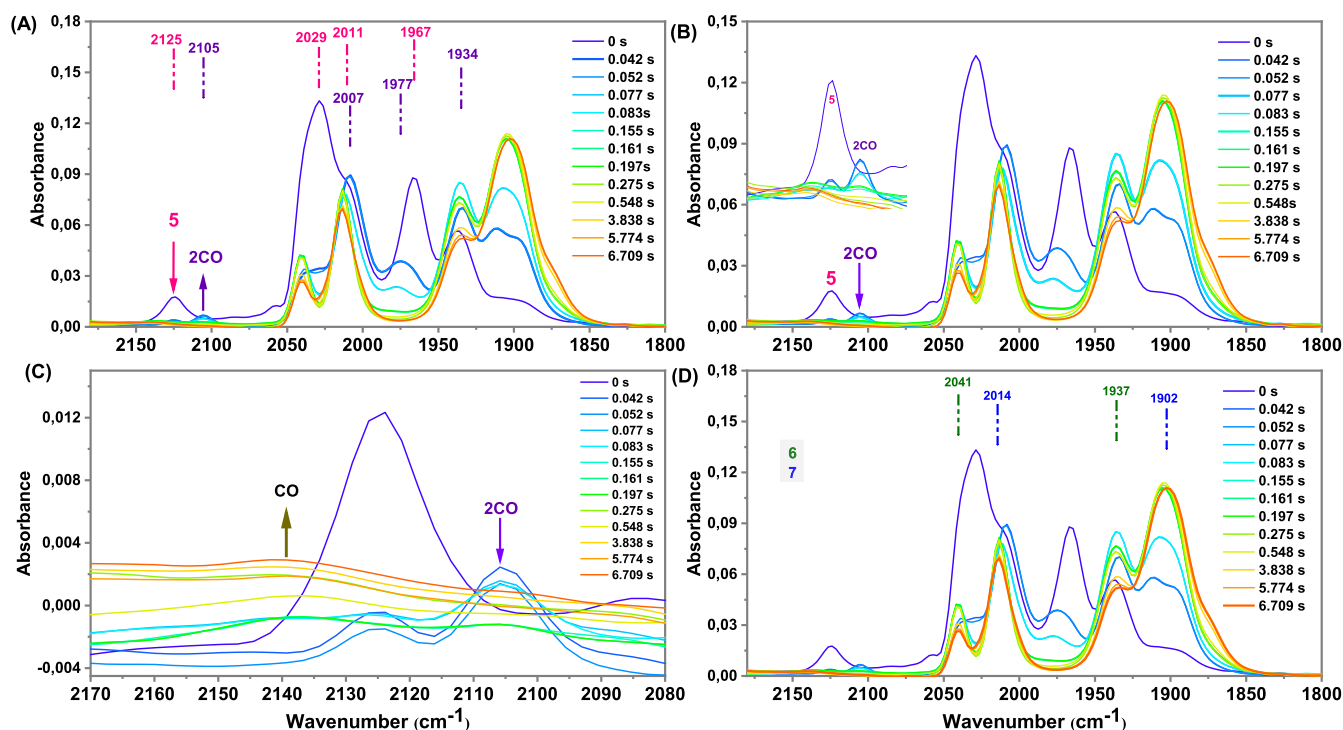


Figure 2. TRIR spectra of **5** (0.7 mM) in CH_3CN solution showing the changes observed upon adding 0.84 mM of CoCp_2^* using stopped-flow mixing. In this figure, the same spectra at different times were highlighted in thick lines. Here, (A) initial species (**5**) and formation of **2CO** (at 42 ms), (B) initiation of the decay of **2CO** (at 77 ms) and its complete decay (at 155 ms), (C) release of the product, CO, from **2CO** intermediate, and (D) products (**6** and **7**) were observed after the reaction. Here, we have used a 500 μm spacer in our observation cell. The concentrations mentioned here are the corresponding concentrations in the FTIR observation cell.

discussed. We believe this study will help the community in complementing the current mechanistic understanding of the $\text{Re}(\text{bpy})(\text{CO})_3\text{X}$ ($\text{X} = -\text{Cl}/-\text{Br}$)-catalyzed CO_2RR .

RESULTS AND DISCUSSION

To put this study into the context of the current understanding of the CO_2RR mechanistic cycle catalyzed by this class of catalysts, we will start this section with a brief overview of the work that has been done to elucidate the catalytic cycle and the important steps that remained to be solved.

According to the well-recognized mechanism of eCO_2RR (Figure 1), **1** undergoes two-electron reduction and subsequent halide loss to generate the catalytically active species, 2^- . Subsequently, binding of CO_2 to 2^- followed by protonation leads to the formation of the corresponding hydroxycarbonyl intermediate, **4**. Further protonation of **4**, accompanied by the loss of a water molecule, leads to the formation of a cationic tetracarbonyl species, **5**. **5** then undergoes further reduction to yield a reduced tetracarbonyl (**2CO** or **2**) and releases CO as a product. Finally, another one-electron reduction regenerates the initial 2^- species, closing the catalytic cycle.³¹ On the other hand, under photochemical conditions, $[\text{Re}(\text{bpy})(\text{CO})_3]^0$ (**2**) is formed after one-electron reduction of **1** and subsequent halide loss. CO_2 then binds to **2** and undergoes one electron reduction followed by protonation to generate the corresponding hydroxy carbonyl intermediate (**4**).³² The rest of the mechanistic cycle is the same as the corresponding eCO_2RR (Figure 1 and Scheme 2). Previously, the hydroxy carbonyl intermediate (**4**) was detected in substrate binding (CO_2) studies with 2^- under chemical conditions utilizing stopped-flow mixing coupled to TRIR.³⁶ Recently, the hydroxy

carbonyl intermediate (**4** and $4_{\text{Ru-Re}}$) was also observed during the mechanistic studies with this catalyst and the famous $\text{Ru}(\text{II})-\text{Re}(\text{I})$ supramolecular assembly ($\text{Ru}-\text{Re}$) under photochemical conditions utilizing cold-spray ionization mass spectrometry and time-resolved FTIR (TRIR) coupled to laser flash photolysis, respectively.^{34,35} Using vibrational sum frequency generation spectroscopy and FTIR-SEC, $\text{S}_{\text{Mn}}[\text{Mn}(\text{bpy-R})(\text{CO})_4]^+$ has been observed in situ under catalytic conditions using the analogous Mn tricarbonyl complexes having bpy and N-heterocyclic carbene ligands, respectively.^{39,40} However, the attempt at in situ detection of **2CO** (Figure 1A), which is an important intermediate in both eCO_2RR and photo- CO_2RR , has failed as this species is proposed to be very short-lived at room temperature.^{38,41} Therefore, it creates uncertainty about **2CO**'s existence in the mechanistic cycle, suggesting that the product (CO) release might be coupled to the reduction of **5**. Previously, the involvement of **5** in the catalytic cycle was established by Grice et al. They synthesized **5** and were successful in showing that this complex also acts as an electrocatalyst for the selective generation of CO from CO_2 . Interestingly, **5** performed eCO_2RR at $\sim 300\text{--}350$ mV less overpotential relative to the parent halide complex but with poorer $i_{\text{cat}}/i_{\text{p}}$ ratios.³⁸

Another long-standing unresolved mystery lies in the poor photo- CO_2RR performance of these types of catalysts in CH_3CN , an exceptional solvent, regularly employed in both photo-/ eCO_2RR .³⁵ Iitani and co-workers suggest that the higher binding affinity of CH_3CN might suppress the formation of the TEOA- CO_2 adduct, an important intermediate that helps in achieving higher photocatalytic activity by capturing CO_2 in DMF-TEOA mixed solvent. Again, the inclusion of TEOA into the C-N bond of CH_3CN forming

corresponding iminoester species was also suggested as the possible reason for its poor reactivity.²¹ However, the exact reason is still unclear. All of these questions motivated us to explore the product release step of the CO₂RR catalytic cycle (Figure 1 and Scheme 2) in CH₃CN.

Synthesis and Characterization of [Re(bpy)(CO)₄]OTf (5). 5 was synthesized following the method reported by Rillema and co-workers with slight modifications⁴² (see the experimental section, Supporting Information) and fully characterized by NMR (¹H, ¹³C, and ¹⁹F), FTIR, and HRMS (Figures S1–S4, S19). 5 possess C_{2v} symmetry and in CH₃CN, it shows four CO vibrations at 2125 cm⁻¹ (A₁ mode, for cis carbonyls), 2029 cm⁻¹ (B₁ mode), 2011 cm⁻¹ (another A₁ mode for trans carbonyls), and 1967 cm⁻¹ (B₂ mode).⁴³ Previously, it has been shown that the cyclic voltammogram of 5 under an argon atmosphere consists of one irreversible (at -1.15 V vs SCE) and two quasi-reversible waves (at -1.27 and -1.42 V, vs SCE) in CH₃CN. 5 serves as a catalyst for eCO₂RR and shows the electrocatalytic response at ~-1.53 V (vs SCE).³⁸ To follow the kinetics of the electron transfer step under pure chemical conditions (5 to 2 or 2CO), we employed stopped-flow mixing of 5 and a chemical reductant and followed the kinetics by monitoring the intense and characteristic CO vibrations. Stopped-flow mixing coupled to FTIR was previously utilized to monitor the CO₂ and H⁺ binding kinetics to the doubly reduced Re-bipyridine complex (2⁻).^{36,37} In our work, using the cyclic voltammograms of 1, we have used decamethyl cobaltocene (CoCp₂^{*}, -1.56 V vs SCE) as the reductant.

TRIR Experiments Identifying a 2CO Intermediate.

Stopped-flow TRIR measurements were performed by mixing 0.7 mM 5 with 0.84 mM CoCp₂^{*} in CH₃CN (Figure 2). Note that the concentrations mentioned here are the corresponding concentrations in the observation cell. The data (Figure 2) show that 5 reacts very fast with CoCp₂^{*}, showing a mixture of species already present in the initial spectrum (at 0 s). The vibrational bands corresponding to 5 show subsequent rapid decay with the generation of other vibrational bands. Looking carefully, we observed that, at 42 ms, some new bands arise at 2105 cm⁻¹, 2041 cm⁻¹ (br), 2007 cm⁻¹, 1977 cm⁻¹ (br), 1934 cm⁻¹, and ~1902 cm⁻¹ (br) (Figure 2A). After comparing with the reported CO frequencies of some intermediates, we concluded that the vibrational spectrum at 42 ms consists of a mixture of 5, [Re(bpy)(CO)₃(CH₃CN)]⁺ (7, $\nu_{\text{CO}} = 2041 \text{ cm}^{-1}, 1937 \text{ cm}^{-1}$), [Re(bpy)(CO)₃(CH₃CN)]⁰ (6, $\nu_{\text{CO}} = 2014 \text{ cm}^{-1}, 1902 \text{ cm}^{-1}$),³⁸ and a previously uncharacterized species having vibrational bands around 2105, 2007, 1977, and 1934 cm⁻¹. The observation of vibrational bands near 2105 cm⁻¹ is a clear indication of the latter being a tetracarbonyl species.⁴² To extract the vibrational spectrum of the reduced Re-tetracarbonyl species (2CO), we deconvoluted the spectrum at 42 ms utilizing the reported IR frequencies of 5, 6, and 7 (Figures S8, S10) and applied the deconvolution to all the spectra to obtain the time profiles (Figure S9). We calculated the vibrational frequency of 2CO using density functional theory calculations employing unrestricted B3LYP functional and Def2-TZVP basis sets (Figures S6–S7).⁴⁴ The calculated ν_{CO} values and intensities are in good agreement with our observations (Table 1). A mere 20 cm⁻¹ downshift of the CO stretching frequency indicates that the reduction is ligand-based. The highest occupied molecular orbital of 2CO, obtained from density-functional theory (DFT) calculations, revealed that the extra electron is localized onto the bpy ligand

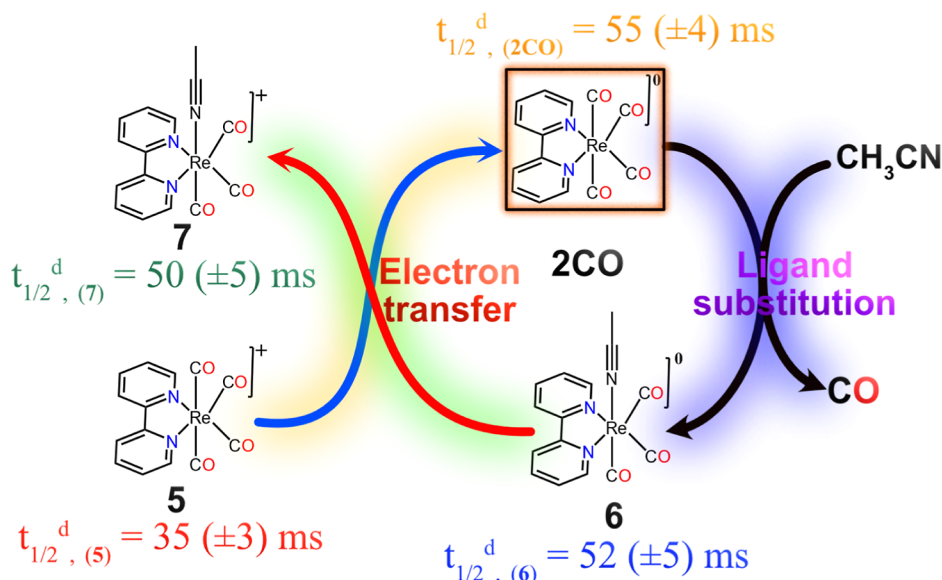
Table 1. Experimental and Calculated (b3lyp/Def2-tzvp with GD3BJ Dispersion Correction) Vibrational Frequencies of the Species Discussed in this Paper^a

species	experimental vibrational frequencies (cm ⁻¹)	calculated vibrational frequencies (cm ⁻¹)
[Re(bpy)(CO) ₄] ⁺ (5)	2125, 2029, 2011, 1967	2138, 2020, 2010, 1963
[Re(bpy)(CO) ₄] ⁰ (2CO)	2105, 2007, 1977, 1934	2118, 1993, 1973, 1924
[Re(bpy)(CO) ₃ (CH ₃ CN)] ⁰ (6)	2014, 1902	2015, 1897, 1887
[Re(bpy)(CO) ₃ (CH ₃ CN)] ⁺ (7)	2041, 1937	2045, 1934, 1926

^aThe experimental frequencies of 5, 6, and 7 have been reported elsewhere.³⁸

(Figure S11), which is in line with the previous report by Kubiak and co-workers. As a result of this ligand-based reduction, the vibrational bands at ~1604 cm⁻¹ (for the bpy ligand) are expected to shift to ~1554 cm⁻¹ after reduction.⁴¹ Comparing the FTIR spectra of 5 to the intermediate spectra (at 42 ms) shows a similar shift in the ν_{bpy} vibration (Figure S12). All of these observations advocate the generation of 2CO having the above-mentioned vibrations (Figure S10). This species signal decreases after 77 ms and completely disappears at 155 ms, showing a half-life of ~55 ms (Figure 2B) under these conditions.

As 2CO started to decay, a broad band centered around 2140 cm⁻¹ appeared and gained intensity as 2CO decayed completely (Figure 2C). This band corresponds to dissolved CO in CH₃CN (Figure S13). The apparent rate constant for the release of CO ($k_{1,(\text{CO})}$) is ~15 (±3) s⁻¹, which matches well with the apparent rate constant for the disappearance of 2CO ($k_{-1,(2\text{CO})} = 18 (\pm 2) \text{ s}^{-1}$), solidifying further that 2CO is the product-releasing intermediate (Figure S14). Thus, these TRIR data suggest that upon one-electron reduction, 5 converts into 2CO, which has a half-life of ~55 ms at room temperature (295 K), and the consumption of 2CO is followed by the release of CO. Note that the characteristic vibrational features of the 2CO species were also observed during the stopped-flow TRIR experiments performed by varying the concentrations of 5 and CoCp₂^{*} (vide infra, Figures S15–S21). The identity of the product (CO)-releasing intermediate during the Re(bpy)(CO)₃Cl-catalyzed eCO₂RR/photo-CO₂RR has since long been debated.^{30–32,38,45} 2CO is a proposed common intermediate present in the mechanistic cycle of both eCO₂RR/photo-CO₂RR.^{31,32} However, the transient nature of 2CO at room temperature made it difficult to observe it under operando SEC experiments.³⁸ This leads to the assumption that 2CO may not be present in the catalytic cycle. Instead, the reduction of 5 and the release of the product (CO) may occur as a concerted step in the mechanistic cycle. However, our TRIR data conclusively prove that the product (CO) release in Re(bpy)(CO)₃Cl-catalyzed eCO₂RR/photo-CO₂RR happens only after the formation of the reduced tetracarbonyl species (2CO), which was hypothesized before though not observed experimentally. It is interesting that the bipyridine-centered reduction promotes the CO release in the tetracarbonyl species. To understand more, we looked into the optimized geometry of the [Re(bpy)(CO)₄]⁺ and [Re(bpy)(CO)₄]⁰ species. It appears that the axial Re–CO bond elongated more than the other bonds after the reduction

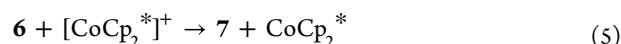
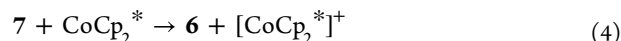
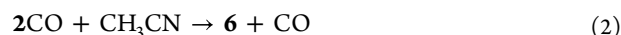
Scheme 1. Proposed Mechanism for the Electron-Transfer-Catalyzed Ligand Substitution reaction^{38a}

^aThe transient intermediate, 2CO, that was observed in our study has been highlighted here. Here, the half-lives for the formation ($t_{1/2}^f$) and decay ($t_{1/2}^d$) are obtained from the reaction of 0.7 mM **5** with 0.84 mM CoCp_2^* (Figure S8). Please note that these half-life values are highly dependent on the reaction conditions due to the competition between direct reduction and autocatalysis.

(Figure S22), facilitating the CO release. The calculated $\Delta G_{\text{reaction}}$ for the release of CO from both $[\text{Re}(\text{bpy})(\text{CO})_4]^+$ and $[\text{Re}(\text{bpy})(\text{CO})_4]^0$ species revealed that the former reaction is ca. 6 kcal mol⁻¹ less favorable than the latter (Table S1).

The removal of CO from 2CO will generate the radical species, $[\text{Re}(\text{bpy})(\text{CO})_3]^\bullet$, which can either dimerize to form $[\text{Re}(\text{bpy})(\text{CO})_3]_2$ or could generate solvent-bound radical species, $[\text{Re}(\text{bpy})(\text{CO})_3(\text{CH}_3\text{CN})]^0$ (**6**). A detailed experimental and theoretical study made by Fujita and Muckerman demonstrates that the solvent-bound (THF in this case) radical species is more stable than the five-coordinate $[\text{Re}(\text{bpy})(\text{CO})_3]^\bullet$ species, resulting in almost nine orders slower dimerization rate (by blocking the available site for dimerization) compared to the typical metal radicals like $[\text{Re}(\text{CO})_5]^\bullet$.⁴⁶ Thus, in our experiments, we expected to observe only **6** as the product after the reaction but to our surprise, the accumulation of the oxidized solvento species, $[\text{Re}(\text{bpy})(\text{CO})_3(\text{CH}_3\text{CN})]^+$ (**7**), as one of the products was also observed. The detection of the ligand substituted product of **5**, $[\text{Re}(\text{bpy})(\text{CO})_3(\text{CH}_3\text{CN})]^+$, as one of the reduction products is very intriguing as **5** is very stable in CH_3CN ⁴⁷ and does not show any sign of conversion to **7** upon keeping it in solvent for hours (Figure S23). During the studies of the excited state dynamics of $[\text{Re}(\text{LL})(\text{CO})_4]^+$ complexes (where LL is bpy, 4,4'-dimethyl bpy, and 1,10-phenanthroline) using TRIR, Schoonover and co-workers observed the accumulation of oxidized solvento species (7-DCE, $[\text{Re}(\text{bpy})(\text{CO})_3(\text{DCE})]^+$) species as the photodissociation product. However, they mistakenly assigned the product to be $[\text{Re}(\text{bpy})(\text{CO})_3(\text{DCE})]^0$ (DCE = dichloroethane) although the FTIR bands corresponding to the photoreduced product are aligned with $[\text{Re}(\text{bpy})(\text{CO})_3(\text{DCE})]^+$.⁴³ Thus, the mechanism of the formation of **7** from **5** under the photoreduction conditions remains unexplained. Nevertheless, the formation of a solvento species from an oxidized tetracarbonyl species under electrochemical conditions was

well documented in the literature for group 6 metal carbonyl complexes.⁴⁸ This reactivity was termed an electrode-catalyzed ligand substitution reaction. Recently, Kubiak and Bocarsly group reported similar reactivity for the analogous Re and Mn bipyridine tetracarbonyl complexes under electrochemical controls.^{38,41} Kubiak and co-workers also observed the accumulation of the oxidized solvento species (**7**) in the presence of a substoichiometric concentration of potassium-intercalated graphite (KC_8), i.e., under chemical control and renamed the mechanism as electron-transfer catalyzed ligand substitution reaction.³⁸ In a typical electron transfer-catalyzed ligand substitution reaction, the reduction of the oxidized tetracarbonyl complex (by either electrochemical or chemical reduction means) generates the reduced tetracarbonyl species (2CO), which then loses one CO ligand and binds one solvent molecule rapidly, forming the reduced solvento species (**6**). As soon as **6** is formed, it behaves as a reducing agent reacting with **5**, yielding **7** and 2CO (Scheme 1), and this autocatalytic cycle continues until the complete consumption of **5**.



Electron-Transfer-Catalyzed Ligand Substitution Reaction. The observation of **7** as one of the products in our TRIR study (under pure chemical reduction) is fascinating, and we were interested in understanding the mechanistic and kinetic aspects of this electron-transfer-catalyzed ligand substitution reaction. Previously, these types of reactions were studied under electrochemical controls for group 6 and 7 metal tetracarbonyl complexes.^{38,41,48–52} Although Grice et al. were able to see the signature of **7** under chemical conditions

using substoichiometric KC_8 concentrations, they did not observe **6** during this reaction. They also reported that a complete conversion of **5** to **7** requires the presence of an electrolyte (tetra butyl ammonium hexafluorophosphate, in their case) as an electron transfer mediator. In our case, no dedicated electron transfer mediator was required to drive the reaction toward completion, even with substoichiometric amounts of CoCp_2^* . We are also curious about any possible effect of the concentration of the reactants on the kinetics of the reaction. Therefore, we performed several TRIR studies by varying the relative concentrations of CoCp_2^* and **5**. In these experiments, we loaded a fixed concentration of both of them into the stopped-flow instrument and changed their relative concentrations in the IR observation cell by mixing them at different volumetric ratios ($5/\text{CoCp}_2^* = 1:1$ to $4:1$). This helped us to achieve a better signal-to-noise ratio without losing the essence of the substoichiometric reductant conditions. To be concise, we will discuss the kinetic results only under low concentration (0.5 mM) and high concentration (3 mM) of **5** and CoCp_2^* , and the rest (with 2 mM concentration) are discussed in the [Supporting Information](#) (Figures S27–S28). The higher energy vibrational bands of **5**, **6**, and **7** (2029 & 2011 cm^{-1} for **5**, 2014 cm^{-1} for **6**, and 2041 cm^{-1} for **7**) are close to each other, making the corresponding kinetic analysis difficult using those traces. Therefore, we chose the traces of other vibrational bands like 1967 and 2125 cm^{-1} for **5**, 1937 cm^{-1} for **7**, and 1902 cm^{-1} for **6** for the kinetic analysis.

At Low Concentration Regime (with 0.5 mM Stock Solutions of **5 and CoCp_2^*).** The TRIR spectra presented in [Figure 3](#) show the changes in the vibrational bands indicating

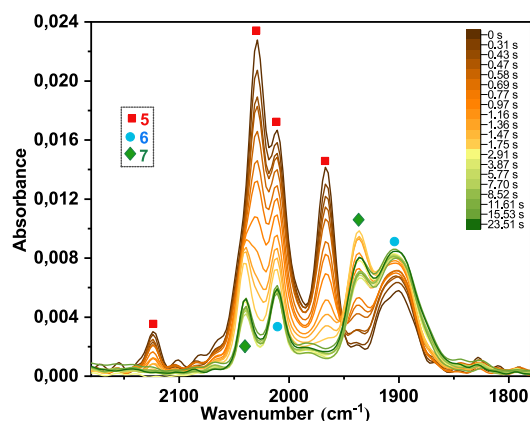


Figure 3. TRIR spectra of the reaction (after stopped-flow mixing) of 0.25 mM **5** with 0.25 mM CoCp_2^* in CH_3CN (mentioned concentrations are at the IR observation cell). The spectra show the time evolution of different species **5**, **6**, and **7**. Here, we have used 0.5 mM each of **5** and CoCp_2^* as the stock solution and performed the mixing at a 1:1 ratio.

the formation of new species from **5** after mixing 0.25 mM CoCp_2^* to 0.25 mM **5** in CH_3CN . Note that the concentrations mentioned here reflect the concentrations at the IR observation cell. At these lower concentrations, the conversion of **5** to **6** is slower, as can be expected. The possible reactions ongoing in our case are shown above. Some **6** is present already in the initial spectra, however, for reasons we cannot explain.

This reduced tetracarbonyl species, **2CO**, is transient at room temperature as evident from its short half-life of ~ 55 ms. Subsequently, CO (product) release and the binding of the solvent molecule to the five-coordinated radical species, $[\text{Re}(\text{bpy})(\text{CO})_3]^*$, is also reported to have very fast kinetics (eq 1 and 2, [Scheme 1](#)).⁴⁶ Once **6** is generated, it reacts with **5**, forming **7** and **2CO**, and the latter further forms **6** upon solvent binding (eq 3). In this scheme, the overall rate of the reaction is limited by eq 3 (which is slower compared to the reactions mentioned in eqs 1 and 2), and the corresponding kinetics, captured by the employed technique, are utilized here for the analysis.

According to the mechanism of the electron-transfer-catalyzed ligand substitution reaction, as soon as a small amount of **6** is generated, it readily starts the autocatalytic reaction, generating both **6** and **7** and it can be assumed that the concentration of **6** in eq 3 ([Scheme 1](#)) is much smaller than the concentration of **5** (also evident from the kinetic traces in [Figure 4B](#)), which allows us to use pseudo-first-order exponential rate equations to analyze the kinetics of the corresponding reactions.

In the reaction of 0.25 mM **5** with 0.25 mM CoCp_2^* , the trace at 1967 cm^{-1} (corresponding to **5**) decays, with an apparent rate constant ($k_{-1,(5)}$) of 1.2 s^{-1} . Please note that these apparent rate constant values are highly dependent on the reaction conditions and carry $\sim 10\%$ error in their values. More than one exponential function was needed to fit the traces at 1902 cm^{-1} (**6**) and 1937 cm^{-1} (**7**) among which the initial rate constant of their formation is very similar to the rate constant of the decay of **5**, which is expected according to eq 3 ([Figure 4A,B](#)). At the end of the reaction (30 s), both **6** and **7** remain because **5** has been consumed and the CoCp_2^* potential is similar to the **7/6** potential (vide supra). Thus, the slower evolution ($t > 1$ – 2 s) is attributed to equilibration between **6** and **7**. However, the steady-state concentration of **6** is smaller compared to **7**, evident from the corresponding ΔA values.

Upon increasing the relative concentration ratios ($5/\text{CoCp}_2^*$) to 0.33 mM/0.16 mM (2:1) and 0.375 mM/0.125 mM (3:1) ([Figure S24–S25](#)), a similar kinetic behavior of the 1937 cm^{-1} trace was observed. It grows with similar apparent rate constants ($k_{1,(7)} = 0.6$ s^{-1}) as that of the decay of **5** ($k_{-1,(5)} = 0.7$ s^{-1}). At a longer time scale, **7** decays almost 70% and 25% from its highest steady-state concentration (comparing the ΔA at 1937 cm^{-1} , [Figure S25](#)) as we moved from a 2:1 to a 3:1 ratio, respectively. We believe that the reaction of **7** with the unreacted CoCp_2^* (due to the autocatalytic pathway) is responsible for the conversion of **7** to **6** (eq 4). The observed apparent rate constant for the formation of **6** is probably an average of its formation following eqs 2 and 4. As we moved to a 4:1 ratio (0.4 mM/0.1 mM), the reaction became even slower and only the growth of **7** was captured without any considerable decay ([Figure 4D](#)). The apparent rate constant of the formation of **6** and **7** is ~ 0.3 s^{-1} , which aligns with the decay rate constant of 0.2 s^{-1} for **5**. As we moved toward the substoichiometric concentrations of the CoCp_2^* (from 1:1 ratio to 4:1 ratio), the fitting of the kinetic traces using single exponential functions became poorer ([Figures 4](#) and [S25](#)) and the traces feature a sigmoidal behavior, characteristic of an autocatalytic reaction. We were successful in reproducing these sigmoidal features using a consecutive reaction (eqs 2 and 3) kinetic model (see the [Supporting Information](#), [Figure S26](#)). The rate constants extracted from the experimental traces at

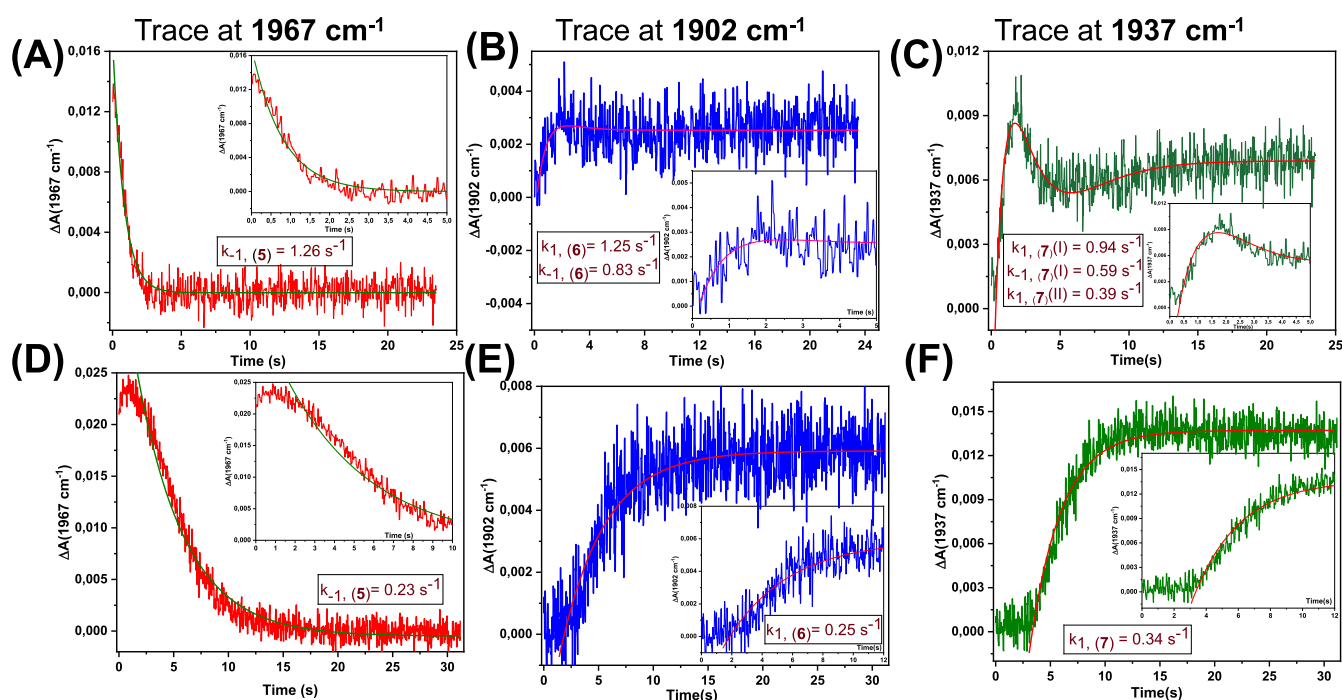


Figure 4. Kinetic traces of the vibrational bands corresponding to 5 (1967 cm^{-1}), 6 (1902 cm^{-1}), and 7 (1937 cm^{-1}) observed during the reaction between 5 and CoCp_2^* at different concentrations. (A–C) 0.25 mM/0.25 mM and (D–F) 0.4 mM/0.1 mM. These concentrations are the concentrations at the IR observation cell. Here, we used 0.5 mM each of 5 and CoCp_2^* as the stock solution and performed the mixing at 1:1 and 4:1 ratios. k_1 and k_{-1} represent the apparent rate constant for the formation and decay of the species, respectively.

the lower concentration regime (0.5 mM case with varying ratios of 5 and CoCp_2^*) and the corresponding concentrations of 5 and CoCp_2^* were used as inputs during the simulations. The behavior of the simulated kinetic traces at the shorter time scale matches perfectly well with the corresponding experimental ones. However, at a longer time scale, some deviations were observed because in our simulations, we did not include the side reactions of 6 and 7 with $[\text{CoCp}_2^*]^+$ and CoCp_2^* (eqs 4 and 5).

These concentration dependence experiments at the low concentration regime of CoCp_2^* suggest that the generation of a small amount of 6 is sufficient to start the autocatalytic pathways but the initial accumulation of 6 following eqs 1 and 2 is too fast to observe in our instrument. Therefore, the kinetics we are observing here mainly follow eq 3 (4 and 5 for the slow reactions with CoCp_2^* and $[\text{CoCp}_2^*]^+$) as formation rates of both 6 and 7 are almost equal to the decay of 5.

In the previous chemical reduction experiment using KC_8 , the authors used 50 mM 5 and observed only 7 as the product without observing any signature of 6 although we did see 6 at lower concentrations. Thus, we were curious if there is any effect of the concentration of either 5 or CoCp_2^* in the product distributions. This question led us to perform more experiments with higher concentrations of 5 and CoCp_2^* (vide supra, Figures S27–S28, 5, and S29–S30) like 2 and 3 mM (stock concentrations) with varying mixing ratios during the stopped-flow TRIR experiments. In the following sections, we will discuss the results obtained from the experiments performed with the 3 mM case with varying mixing ratios, and the 2 mM case is discussed briefly in the Supporting Information.

At High Concentration Regime (with 3 mM Stock Solutions of 5 and CoCp_2^*). At the equal concentration of CoCp_2^* and 5 (1.5 mM each at the observation cell), we saw a

mixture of 2CO, 5, and 7 at the very initial spectra of the TRIR data (Figures S20 and S29). Then, 6 accumulates rapidly followed by its decay (probably following eq 5). As the initial spectrum is a mixture of at least three species, kinetic analysis is complex to pursue. The electron-catalyzed ligand substitution reaction is reported to be pronounced at a substoichiometric concentration of the reductant. Therefore, we analyze the kinetic traces obtained from the stopped-flow TRIR experiments performed at higher mixing ratios: 2:1 (2/1 mM), 3:1 (2.25/0.75 mM), and 4:1 (2.4 mM/0.6 mM). The TRIR spectra of the reaction between 5 and CoCp_2^* at these concentrations show the generation of 7 in a considerable amount at the very beginning (Figure S29) and with increasing the relative ratios of the reactants, less amount of 7 was seen in the initial spectra.

At a 2:1 ratio (5: CoCp_2^* = 2 mM/1 mM), we can resolve the formation of 7. The kinetic traces at 1902 and 1937 cm^{-1} give the apparent rate constants, 5.3 and 7.0 s^{-1} , for the formation of 6 and 7, respectively, which are close to each other and match well with the apparent decay rate constant of 5 (1967 cm^{-1} trace, Figure 5A–C). Note that 5 will be consumed through parallel reactions i.e., direct reduction with CoCp_2^* and the autocatalytic pathway. Later, 6 starts to decay with a rate constant of 0.3 s^{-1} , presumably upon its reaction with remaining $[\text{CoCp}_2^*]^+$, contributing to a small increase in the concentration of 7 (Figure 5A–C). The traces at 1902 and 1937 cm^{-1} at all of the concentration ratios have slower components due to the interconversion between 6 and 7 (eqs 4 and 5). At this high concentration regime, the trace at 1967 cm^{-1} (5) was also affected due to the large absorbance of the 1937 cm^{-1} peak (Figures 5, and S29). The apparent rate constant values of the growth over a longer time were small and remained almost similar in all of the mixing ratios (Figures 5, and S28). We took only the initial decay for our analysis. In

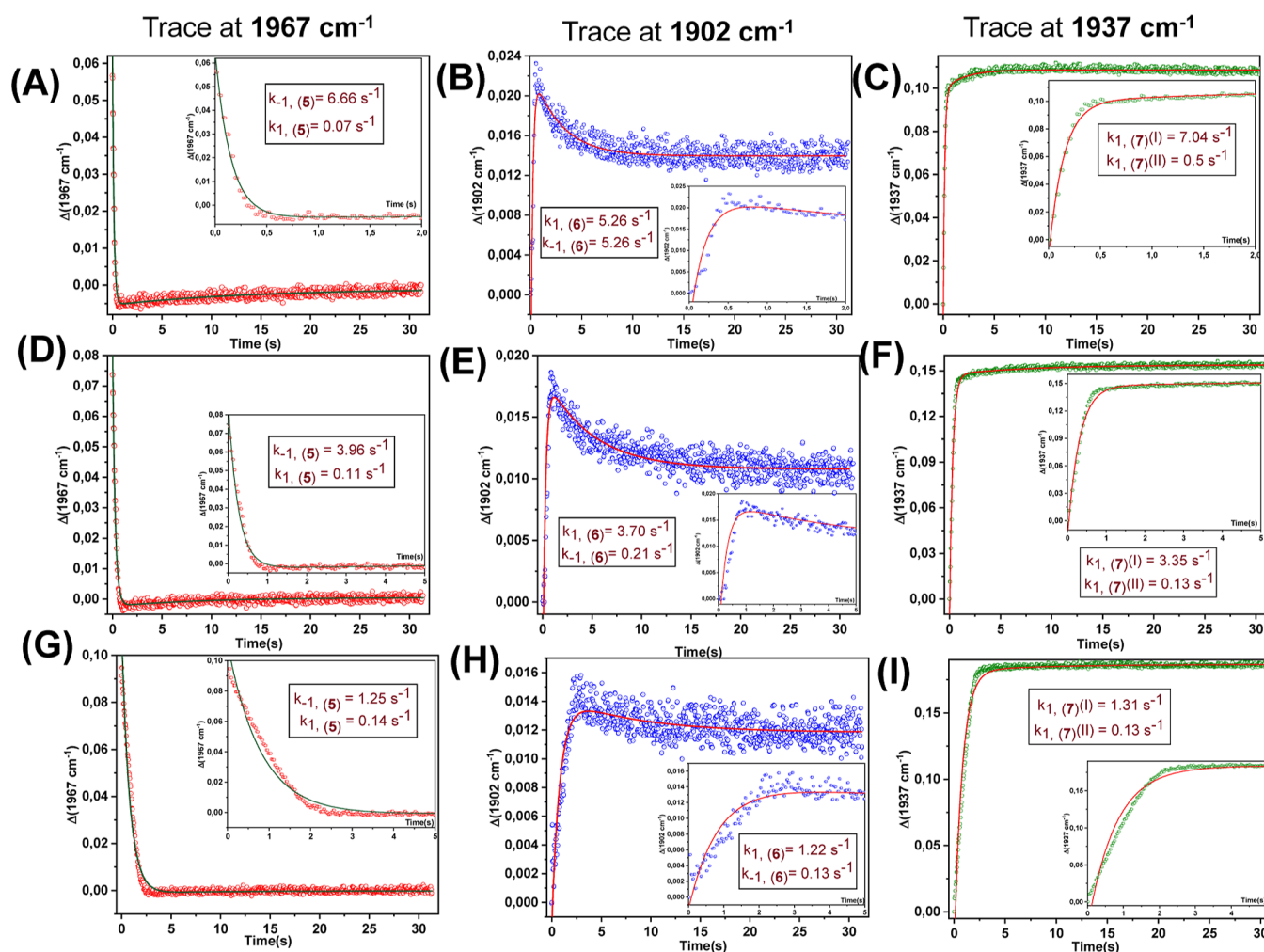


Figure 5. Kinetic traces of the vibrational bands corresponding to 5 (1967 cm^{-1}), 6 (1902 cm^{-1}), and 7 (1937 cm^{-1}) observed during the reaction between 5 and CoCp_2^* at different concentration ratios: (A–C) 2 mM/1 mM, (D–F) 2.25 mM/0.75 mM, (G–I) 2.4 mM/0.6 mM. These concentrations are the concentrations at the IR observation cell. Here, we use 3 mM each of 5 and CoCp_2^* as the stock solution and perform the mixing at 2:1, 3:1, and 4:1 ratios. k_1 and k_{-1} represent the apparent rate constant for the formation and decay of the species, respectively.

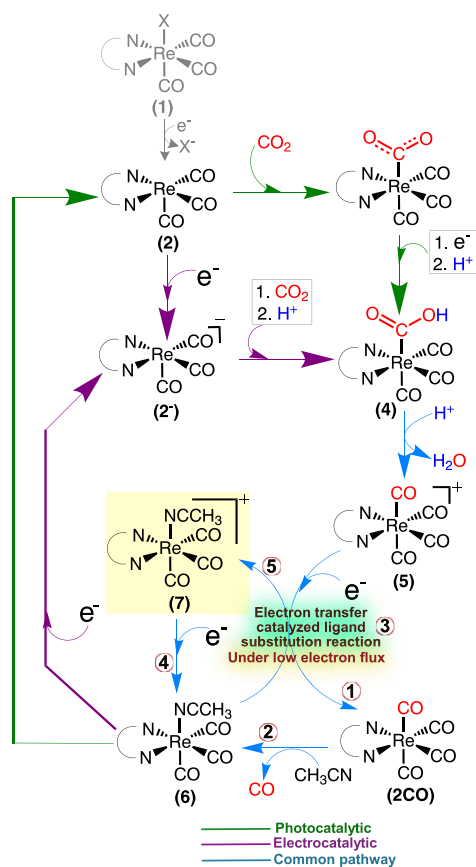
these high concentrations, the 2125 cm^{-1} peak also receives considerable absorbance, we fitted that kinetic trace (Figure S30), and the extracted rate constants also supported our argument. As we increased the concentration of 5 and decreased the concentration of CoCp_2^* in the mixture, similar features of the kinetic traces for 5, 6 and 7 were observed but with a decrease in apparent rate constant (Figures 5 and S29–S30), giving 7 as the final product. In these mixing ratios (2.25 mM/0.75 mM, 2.4 mM/0.6 mM), a very small amount of 6 is formed (almost 1 order of magnitude lower than 7) as evident from the ΔA values shown in Figure 5.

Relevance in View of the CO_2RR Mechanistic Cycle. The inclusion of the 2CO, proposed as a common intermediate to both eCO_2RR and photo- CO_2RR in CH_3CN , in the mechanistic cycle was debated for a long time due to the difficulty in detecting it in conventional FTIR-SEC experiments owing to its presumed short half-life. In this study, utilizing stopped-flow mixing coupled with TRIR, we were able to observe this intermediate at various concentrations and determine its half-life (~ 55 ms) in CH_3CN . Direct product release (CO) from this intermediate was also shown here. Therefore, the modified mechanistic cycle is as follows: the oxidized tetracarbonyl species (5), formed upon

protonation and water removal from the metal-hydroxy carbonyl complex (4), undergoes one-electron reduction to form the 2CO intermediate. 2CO then releases CO spontaneously and generates a mixture of 6 and 7 as the products following the electron-transfer-catalyzed ligand substitution reaction (Scheme 2). In a typical eCO_2RR experiment using the corresponding halide complex, $\text{Re}(\text{bpy})(\text{CO})_3\text{Cl}$, electrocatalysis is performed at a very high cathodic potential relative to that at which 5 does CO_2RR . Thus, the electron-transfer-catalyzed ligand substitution reaction might not affect the electrocatalytic rates and efficiency.²¹ However, when 5 acts as the electrocatalyst, it requires less cathodic potential to release the axial CO and form the active species, 2[−].³⁸ We believe that this applied potential is not large enough to avoid the electron-catalyzed ligand substitution reaction generating 7 as a side product and we propose this is the reason for the lower $i_{\text{cat}}/i_{\text{p}}$ values obtained for 5 compared to the parent halide complex.³⁸

We believe that the electron transfer-catalyzed ligand substitution reaction plays a major role in $\text{Re}(\text{bpy})(\text{CO})_3\text{Cl}$ -catalyzed photo- CO_2RR , as under these conditions, catalysis is limited by the generation of reductant (slower reaction rate for eq 1). After releasing CO, the resultant 6 can react with some

Scheme 2. Modified Mechanistic Cycle of the CO₂RR by the Re(bpy)(CO)₃X (X = -Cl/-Br) Catalyst in CH₃CN^a



^aThe electron-transfer catalyzed ligand substitution reaction and product 7 (highlighted in the yellow box) are much more prominent under low electron flux (limited supply of reducing equivalents).

of the 5 that were not reduced yet and form 7 (Scheme 2). Although this side reaction helps to release CO faster, the resultant product, 7, requires a higher reduction potential relative to 5, to reach the catalytically active species. Under photochemical conditions, the subsequent electron injection is slower compared to that under the electrochemical conditions. That might lead to lower TOF of these catalysts in CH₃CN compared to the same in weakly coordinating solvent, DMF.²¹ However, many other factors also need to be taken into account. One of the major factors is the concentration of the catalyst, as higher catalyst concentration will favor the autocatalytic pathway relative to the CO₂ binding. We were also able to capture this aspect in our experiments, as we observed 6 from the very beginning in the TRIR spectra in the low concentration regime (0.5 mM). However, for the higher concentration case (2, 3, and 4 mM), 7 was observed from the beginning. Thus, all of these considerations must be kept in mind during photo-CO₂RR with these types of catalysts.

CONCLUSIONS

In this study, we utilized stopped-flow mixing combined with TRIR to identify the intermediates involved in the product (CO) release step in Re(bpy)(CO)₃Cl catalyzed CO₂RR, which remained undetected in the previous mechanistic studies. We were able to detect the debated intermediate, for the first time, the reduced Re-tetracarbonyl species ([Re(bpy)-

(CO)₄]⁰, 2CO), and observed product (CO) release directly from it. This confirms definitively that 2CO is part of the mechanistic cycle and suggests that the release of CO does not happen simultaneously with the reduction of the oxidized tetracarbonyl species, 5. Additionally, we demonstrated that the easy release of the product from 2CO is a result of the competitive electron transfer-catalyzed ligand substitution reaction. The stopped-flow FTIR technique used in this study offers improved time resolution, allowing for the detection of intermediates that escape detection in conventional FTIR-SEC experiments. By controlling the concentration of the reductant, this technique can closely mimic both electrocatalytic and photocatalytic conditions. This study also highlights the increasing significance of the electron transfer-catalyzed ligand substitution as reductant concentration decreases, mirroring the slower rate of subsequent reduction steps typically seen in photochemical experiments. Moreover, in a single experiment, we were able to observe all of the species involved in this side reaction along with their kinetic details. The main byproduct of this side reaction, [Re(bpy)(CO)₃(CH₃CN)]⁺ (7), needs a higher reduction potential compared to the intermediate [Re(bpy)(CO)₄]⁺ (5) to form the catalytically active species, [Re(bpy)(CO)₃]⁰ (2). Although the initial activation of the catalyst (Re(bpy)(CO)₃X → 2) is thought to be more energetically demanding than the subsequent reduction process involving product release (5 → 2) and turnover, both reductions require a similar driving force for sustained catalysis due to the easy formation of 7 from 5 via an electron-catalyzed ligand substitution reaction. Consequently, in coordinating solvents like CH₃CN, this reaction could decrease the concentration of the active catalyst if the concentration of reductant is low and its reduction potential is insufficient to revert the catalyst from the oxidized state generated by this side reaction. These conditions are more probable in photo-CO₂RR and may elucidate the catalyst's reduced activity in CH₃CN.

MATERIALS AND METHODS

The Supporting Information file includes details of the materials, experimental procedures, and theoretical calculations.

ASSOCIATED CONTENT

Supporting Information

The Supporting Information is available free of charge at <https://pubs.acs.org/doi/10.1021/acscatal.4c06044>.

Detailed experimental procedures, characterizations of the complex, deconvoluted spectra and additional kinetic traces at different concentrations, calculated vibrational frequencies, and the Cartesian coordinates of the DFT-optimized structures (PDF)

AUTHOR INFORMATION

Corresponding Author

Leif Hammarström – Department of Chemistry—Ångström Laboratories, Uppsala University, Uppsala SE 75120, Sweden; orcid.org/0000-0002-9933-9084; Email: leif.hammarstrom@kemi.uu.se

Authors

Samir Chattopadhyay – Department of Chemistry—Ångström Laboratories, Uppsala University, Uppsala SE 75120, Sweden; orcid.org/0000-0003-4759-0362

Mun Hon Cheah – Department of Chemistry—Ångström Laboratories, Uppsala University, Uppsala SE 75120, Sweden; orcid.org/0000-0001-5732-1524

Reiner Lomoth – Department of Chemistry—Ångström Laboratories, Uppsala University, Uppsala SE 75120, Sweden; orcid.org/0000-0003-2246-1863

Complete contact information is available at:
<https://pubs.acs.org/10.1021/acscatal.4c06044>

Author Contributions

The manuscript was written through the contributions of all authors. Credit: **Samir Chattopadhyay**: Conceptualization (equal); Investigation (lead); Methodology (lead); Formal analysis (lead); Writing—original draft (lead); Writing—review and editing (equal). **Mun Hon Cheah**: Formal analysis (supporting); Writing—review and editing (supporting). **Reiner Lomoth**: Conceptualization (equal); Supervision (equal); Formal analysis (equal); Writing—review and editing (equal). **Leif Hammarström**: Conceptualization (equal); Supervision (equal); Resources (lead); Funding acquisition (lead); Formal analysis (equal); Project administration (lead); Writing—review and editing (equal).

Notes

The authors declare no competing financial interest.

ACKNOWLEDGMENTS

The authors acknowledge financial support from the Wenner-Gren Foundations (grant number: UPD2020-0134 and UPD2021-0112) and the Knut & Alice Wallenberg Foundation (grant number: 2019.0071). The authors also thank the Swedish National Infrastructure for Computing (SNIC) at UPPMAX (snic2022-22-494) and Tetralith (naiss2023-22-1046) for allowing to perform the DFT calculations.

ABBREVIATIONS

CO₂ carbon dioxide
eCO₂RR electrochemical CO₂ reduction reactions
photo-CO₂RR photochemical CO₂ reduction reactions
SHE standard hydrogen electrode
HER hydrogen evolution reaction
bpy 2,2'-bipyridine
CH₃CN acetonitrile
DCE dichloroethane
TRIR time-resolved infrared spectroscopy
DFT density-functional theory

REFERENCES

- (1) Chen, C.; Khosrowabadi Kotyk, J. F.; Sheehan, S. W. Progress toward Commercial Application of Electrochemical Carbon Dioxide Reduction. *Chem.* **2018**, *4* (11), 2571–2586.
- (2) Appel, A. M.; Bercaw, J. E.; Bocarsly, A. B.; Dobbek, H.; DuBois, D. L.; Dupuis, M.; Ferry, J. G.; Fujita, E.; Hille, R.; Kenis, P. J. A.; et al. Frontiers, Opportunities, and Challenges in Biochemical and Chemical Catalysis of CO₂ Fixation. *Chem. Rev.* **2013**, *113* (8), 6621–6658.
- (3) Zhang, S.; Fan, Q.; Xia, R.; Meyer, T. J. CO₂ Reduction: From Homogeneous to Heterogeneous Electrocatalysis. *Acc. Chem. Res.* **2020**, *53* (1), 255–264.
- (4) Yao, B.; Xiao, T.; Makgae, O. A.; Jie, X.; Gonzalez-Cortes, S.; Guan, S.; Kirkland, A. I.; Dilworth, J. R.; Al-Megren, H. A.; Alshihri, S. M.; et al. Transforming carbon dioxide into jet fuel using an organic combustion-synthesized Fe-Mn-K catalyst. *Nat. Commun.* **2020**, *11* (1), 6395.
- (5) Sahin, S.; Lemaire, O. N.; Belhamri, M.; Kurth, J. M.; Welte, C. U.; Wagner, T.; Milton, R. D. Bioelectrocatalytic CO₂ Reduction by Mo-Dependent Formylmethanofuran Dehydrogenase. *Angew. Chem., Int. Ed.* **2023**, *62* (45), No. e202311981. (accessed 2024/04/23)
- (6) Gotico, P.; Halime, Z.; Aukaaloo, A. Recent advances in metalloporphyrin-based catalyst design towards carbon dioxide reduction: from bio-inspired second coordination sphere modifications to hierarchical architectures. *Dalton Trans.* **2020**, *49* (8), 2381–2396.
- (7) Jiang, C.; Nichols, A. W.; Machan, C. W. A look at periodic trends in d-block molecular electrocatalysts for CO₂ reduction. *Dalton Trans.* **2019**, *48* (26), 9454–9468.
- (8) Li, Y.; Gomez-Mingot, M.; Fogeron, T.; Fontcave, M. Carbon Dioxide Reduction: A Bioinspired Catalysis Approach. *Acc. Chem. Res.* **2021**, *54* (23), 4250–4261.
- (9) Benson, E. E.; Kubiak, C. P.; Sathrum, A. J.; Smieja, J. M. Electrocatalytic and homogeneous approaches to conversion of CO₂ to liquid fuels. *Chem. Soc. Rev.* **2009**, *38* (1), 89–99.
- (10) Das, B.; Thapper, A.; Ott, S.; Colbran, S. B. Structural features of molecular electrocatalysts in multi-electron redox processes for renewable energy – recent advances. *Sustainable Energy Fuels* **2019**, *3* (9), 2159–2175.
- (11) Rotundo, L.; Gobetto, R.; Nervi, C. Electrochemical CO₂ reduction with earth-abundant metal catalysts. *Curr. Opin. Green Sustainable Chem.* **2021**, *31*, 100509.
- (12) Grice, K. A. Carbon dioxide reduction with homogenous early transition metal complexes: Opportunities and challenges for developing CO₂ catalysis. *Coord. Chem. Rev.* **2017**, *336*, 78–95.
- (13) Amanullah, S.; Saha, P.; Nayek, A.; Ahmed, M. E.; Dey, A. Biochemical and artificial pathways for the reduction of carbon dioxide, nitrite and the competing proton reduction: effect of 2nd sphere interactions in catalysis. *Chem. Soc. Rev.* **2021**, *50* (6), 3755–3823.
- (14) Saha, P.; Amanullah, S.; Dey, A. Selectivity in Electrochemical CO₂ Reduction. *Acc. Chem. Res.* **2022**, *55* (2), 134–144.
- (15) Elgrishi, N.; Chambers, M. B.; Wang, X.; Fontcave, M. Molecular polypyridine-based metal complexes as catalysts for the reduction of CO₂. *Chem. Soc. Rev.* **2017**, *46* (3), 761–796.
- (16) Francke, R.; Schille, B.; Roemelt, M. Homogeneously Catalyzed Electroreduction of Carbon Dioxide—Methods, Mechanisms, and Catalysts. *Chem. Rev.* **2018**, *118* (9), 4631–4701.
- (17) Hawecker, J.; Lehn, J.-M.; Zissel, R. Electrocatalytic reduction of carbon dioxide mediated by Re(bipy)(CO)₃Cl (bipy = 2,2'-bipyridine). *J. Chem. Soc., Chem. Commun.* **1984**, No. 6, 328–330.
- (18) Hawecker, J.; Lehn, J.-M.; Zissel, R. Photochemical and Electrochemical Reduction of Carbon Dioxide to Carbon Monoxide Mediated by (2,2'-Bipyridine)tricarboxylchlororhenium(I) and Related Complexes as Homogeneous Catalysts. *Helv. Chim. Acta* **1986**, *69* (8), 1990–2012. (accessed 2024/04/23)
- (19) Smieja, J. M.; Kubiak, C. P. Re(bipy-tBu)(CO)₃Cl—improved Catalytic Activity for Reduction of Carbon Dioxide: IR-Spectroelectrochemical and Mechanistic Studies. *Inorg. Chem.* **2010**, *49* (20), 9283–9289.
- (20) Barrett, J. A.; Miller, C. J.; Kubiak, C. P. Electrochemical Reduction of CO₂ Using Group VII Metal Catalysts. *Trends Chem.* **2021**, *3* (3), 176–187.
- (21) Kuramochi, Y.; Ishitani, O.; Ishida, H. Reaction mechanisms of catalytic photochemical CO₂ reduction using Re(I) and Ru(II) complexes. *Coord. Chem. Rev.* **2018**, *373*, 333–356.
- (22) Jia, X.; Nedzbal, H. S.; Bottum, S. R.; Cahoon, J. F.; Concepcion, J. J.; Donley, C. L.; Gang, A.; Han, Q.; Hazari, N.; Kessinger, M. C.; et al. Synthesis and Surface Attachment of Molecular Re(I) Complexes Supported by Functionalized Bipyridyl Ligands. *Inorg. Chem.* **2023**, *62* (5), 2359–2375.

- (23) Jia, X.; Cui, K.; Alvarez-Hernandez, J. L.; Donley, C. L.; Gang, A.; Hammes-Schiffer, S.; Hazari, N.; Jeon, S.; Mayer, J. M.; Nedzbal, H. S.; et al. Synthesis and Surface Attachment of Molecular Re(I) Hydride Species with Silatrane Functionalized Bipyridyl Ligands. *Organometallics* **2023**, *42* (16), 2238–2250.
- (24) Jia, X.; Stewart-Jones, E.; Alvarez-Hernandez, J. L.; Bein, G. P.; Dempsey, J. L.; Donley, C. L.; Hazari, N.; Houck, M. N.; Li, M.; Mayer, J. M.; et al. Photoelectrochemical CO₂ Reduction to CO Enabled by a Molecular Catalyst Attached to High-Surface-Area Porous Silicon. *J. Am. Chem. Soc.* **2024**, *146* (12), 7998–8004.
- (25) Huffman, B. L.; Bein, G. P.; Atallah, H.; Donley, C. L.; Alameh, R. T.; Wheeler, J. P.; Durand, N.; Harvey, A. K.; Kessinger, M. C.; Chen, C. Y.; et al. Surface Immobilization of a Re(I) Tricarbonyl Phenanthroline Complex to Si(111) through Sonochemical Hydro-silylation. *ACS Appl. Mater. Interfaces* **2023**, *15* (1), 984–996.
- (26) Bhattacharjee, S.; Rahaman, M.; Andrei, V.; Miller, M.; Rodríguez-Jiménez, S.; Lam, E.; Pornrungrroj, C.; Reisner, E. Photoelectrochemical CO₂-to-fuel conversion with simultaneous plastic reforming. *Nat., Synth.* **2023**, *2* (2), 182–192.
- (27) Xu, R.; Si, D.-H.; Zhao, S.-S.; Wu, Q.-J.; Wang, X.-S.; Liu, T.-F.; Zhao, H.; Cao, R.; Huang, Y.-B. Tandem Photocatalysis of CO₂ to C₂H₄ via a Synergistic Rhenium-(I) Bipyridine/Copper-Porphyrinic Triazine Framework. *J. Am. Chem. Soc.* **2023**, *145* (14), 8261–8270.
- (28) Monticelli, S.; Talbot, A.; Gotico, P.; Caillé, F.; Loreau, O.; Del Vecchio, A.; Malandain, A.; Sallustrau, A.; Leibl, W.; Aukauloo, A.; et al. Unlocking full and fast conversion in photocatalytic carbon dioxide reduction for applications in radio-carbonylation. *Nat. Commun.* **2023**, *14* (1), 4451.
- (29) Machan, C. W.; Sampson, M. D.; Chabolla, S. A.; Dang, T.; Kubiak, C. P. Developing a Mechanistic Understanding of Molecular Electrocatalysts for CO₂ Reduction using Infrared Spectroelectrochemistry. *Organometallics* **2014**, *33* (18), 4550–4559.
- (30) Riplinger, C.; Carter, E. A. Influence of Weak Brønsted Acids on Electrocatalytic CO₂ Reduction by Manganese and Rhenium Bipyridine Catalysts. *ACS Catal.* **2015**, *5* (2), 900–908.
- (31) Riplinger, C.; Sampson, M. D.; Ritzmann, A. M.; Kubiak, C. P.; Carter, E. A. Mechanistic Contrasts between Manganese and Rhenium Bipyridine Electrocatalysts for the Reduction of Carbon Dioxide. *J. Am. Chem. Soc.* **2014**, *136* (46), 16285–16298.
- (32) Schneider, T. W.; Ertem, M. Z.; Muckerman, J. T.; Angeles-Boza, A. M. Mechanism of Photocatalytic Reduction of CO₂ by Re(bpy)(CO)₃Cl from Differences in Carbon Isotope Discrimination. *ACS Catal.* **2016**, *6* (8), 5473–5481.
- (33) Benson, E. E.; Kubiak, C. P. Structural investigations into the deactivation pathway of the CO₂ reduction electrocatalyst Re(bpy)(CO)₃Cl. *Chem. Commun.* **2012**, *48* (59), 7374–7376.
- (34) Kamogawa, K.; Kato, Y.; Tamaki, Y.; Noguchi, T.; Nozaki, K.; Nakagawa, T.; Ishitani, O. Overall reaction mechanism of photocatalytic CO₂ reduction on a Re(i)-complex catalyst unit of a Ru(ii)–Re(i) supramolecular photocatalyst. *Chem. Sci.* **2024**, *15* (6), 2074–2088.
- (35) Kou, Y.; Nabetani, Y.; Masui, D.; Shimada, T.; Takagi, S.; Tachibana, H.; Inoue, H. Direct Detection of Key Reaction Intermediates in Photochemical CO₂ Reduction Sensitized by a Rhenium Bipyridine Complex. *J. Am. Chem. Soc.* **2014**, *136* (16), 6021–6030.
- (36) Sampson, M. D.; Froehlich, J. D.; Smieja, J. M.; Benson, E. E.; Sharp, I. D.; Kubiak, C. P. Direct observation of the reduction of carbon dioxide by rhenium bipyridine catalysts. *Energy Environ. Sci.* **2013**, *6* (12), 3748–3755.
- (37) Smieja, J. M.; Benson, E. E.; Kumar, B.; Grice, K. A.; Seu, C. S.; Miller, A. J. M.; Mayer, J. M.; Kubiak, C. P. Kinetic and structural studies, origins of selectivity, and interfacial charge transfer in the artificial photosynthesis of CO. *Proc. Natl. Acad. Sci. U.S.A.* **2012**, *109* (39), 15646–15650.
- (38) Grice, K. A.; Gu, N. X.; Sampson, M. D.; Kubiak, C. P. Carbon monoxide release catalysed by electron transfer: electrochemical and spectroscopic investigations of [Re(bpy-R)(CO)₄](OTf) complexes relevant to CO₂ reduction. *Dalton Trans.* **2013**, *42* (23), 8498–8503.
- (39) Neri, G.; Walsh, J. J.; Teobaldi, G.; Donaldson, P. M.; Cowan, A. J. Detection of catalytic intermediates at an electrode surface during carbon dioxide reduction by an earth-abundant catalyst. *Nat. Catal.* **2018**, *1* (12), 952–959.
- (40) Fernández, S.; Franco, F.; Martínez Belmonte, M.; Friães, S.; Royo, B.; Luis, J. M.; Lloret-Fillol, J. Decoding the CO₂ Reduction Mechanism of a Highly Active Organometallic Manganese Electrocatalyst: Direct Observation of a Hydride Intermediate and Its Implications. *ACS Catal.* **2023**, *13* (15), 10375–10385.
- (41) Kuo, H.-Y.; Tignor, S. E.; Lee, T. S.; Ni, D.; Park, J. E.; Scholes, G. D.; Bocarsly, A. B. Reduction-induced CO dissociation by a [Mn(bpy)(CO)₄] [SbF₆] complex and its relevance in electrocatalytic CO₂ reduction. *Dalton Trans.* **2020**, *49* (3), 891–900.
- (42) Shaver, R. J.; Rillema, D. P. Physical and photophysical properties of rhenium(I) tetracarbonyl complexes. *Inorg. Chem.* **1992**, *31* (20), 4101–4107.
- (43) Bernhard, S.; Omberg, K. M.; Strouse, G. F.; Schoonover, J. R. Time-Resolved IR Studies of [Re(LL)(CO)₄]⁺. *Inorg. Chem.* **2000**, *39* (14), 3107–3110.
- (44) Rotundo, L.; Garino, C.; Priola, E.; Sassone, D.; Rao, H.; Ma, B.; Robert, M.; Fiedler, J.; Gobetto, R.; Nervi, C. Electrochemical and Photochemical Reduction of CO₂ Catalyzed by Re(I) Complexes Carrying Local Proton Sources. *Organometallics* **2019**, *38* (6), 1351–1360.
- (45) Agarwal, J.; Fujita, E.; Schaefer, H. F.; Muckerman, J. T. Mechanisms for CO Production from CO₂ Using Reduced Rhenium Tricarbonyl Catalysts. *J. Am. Chem. Soc.* **2012**, *134* (11), 5180–5186.
- (46) Fujita, E.; Muckerman, J. T. Why Is Re–Re Bond Formation/Cleavage in [Re(bpy)(CO)₃]₂ Different from That in [Re(CO)₅]₂? Experimental and Theoretical Studies on the Dimers and Fragments. *Inorg. Chem.* **2004**, *43* (24), 7636–7647.
- (47) Johnson, F. P. A.; George, M. W.; Hartl, F.; Turner, J. J. Electrocatalytic Reduction of CO₂ Using the Complexes [Re(bpy)(CO)₃L]_n (n = +1, L = P(OEt)₃, CH₃CN; n = 0, L = Cl[−], Otf[−]; bpy = 2,2′-bipyridine; Otf[−] = CF₃SO₃[−]) as Catalyst Precursors: Infrared Spectroelectrochemical Investigation. *Organometallics* **1996**, *15* (15), 3374–3387.
- (48) Miholová, D.; Vlček, A. A. Electrode-catalyzed substitution of M(CO)₄bipy (M = Cr, Mo, W) initiated by reduction. *J. Organomet. Chem.* **1985**, *279* (1), 317–326.
- (49) Doxsee, K. M.; Grubbs, R. H.; Anson, F. C. Decomposition and ligand substitution reaction mechanisms for organometallic radicals. *J. Am. Chem. Soc.* **1984**, *106* (25), 7819–7824.
- (50) Johnson, R.; Madhani, H.; Bullock, J. P. Electrochemical oxidation of Mo(CO)₄(LL) and Mo(CO)₃(LL)(CH₃CN): Generation, infrared characterization, and reactivity of [Mo(CO)₄(LL)]⁺ and [Mo(CO)₃(LL)(CH₃CN)]⁺ (LL = 2,2′-bipyridine, 1,10-phenanthroline and related ligands). *Inorg. Chim. Acta* **2007**, *360* (10), 3414–3423.
- (51) Poli, R.; Owens, B. E.; Linck, R. G. The first electron transfer chain catalyzed ligand substitution reaction that occurs by transforming an odd-electron system into an even-electron one. *J. Am. Chem. Soc.* **1992**, *114* (4), 1302–1307.
- (52) Albers, M. O.; Coville, N. J. Reagent and catalyst induced substitution reactions of metal carbonyl complexes. *Coord. Chem. Rev.* **1984**, *53*, 227–259.